Photoelasticity of crystals from theoretical simulations

A. Erba* and R. Dovesi

Dipartimento di Chimica and Centre of Excellence NIS (Nanostructured Interfaces and Surfaces), Università di Torino, via Giuria 5, IT-10125 Torino (Italy)

(Received 24 May 2013; published 19 July 2013)

An accurate, fully automated, theoretical *ab initio* scheme is presented for the calculation of elasto-optic constants of crystalline systems of any space group of symmetry. The approach is developed within periodic boundary conditions, exploits both translational and point symmetry, and allows for the use of several one-electron Hamiltonians, such as Hartree-Fock, Kohn-Sham, or hybrids. Generalized-gradient functionals are found to improve the agreement with experiments by a factor of 2 with respect to simple local-density ones, commonly used in the literature so far. The explicit dependence of elasto-optic constants from the electric field frequency can be evaluated as well, thus allowing for a closer comparison with experimental data that usually refer to finite frequencies. The relatively large uncertainty associated with experimental measurements, and the use of an electric field with finite wavelength, make the availability of a predictive theoretical scheme particularly helpful in interpreting the photoelastic response of crystals. The proposed scheme, which has been implemented in the CRYSTAL program, proves numerically stable with regard to its computational parameters and accurate with respect to elasto-optic constants of a set of eight crystals for which consolidated experimental values have been reported.

DOI: 10.1103/PhysRevB.88.045121 PACS number(s): 31.15.A−, 78.20.hb, 62.20.de

I. INTRODUCTION

The variation of the refractive index (dielectric constant) with respect to internal or applied strain constitutes the so-called photoelasticity, or elasto-optics, of a crystal.[1] Brillouin scattering, that is, the interaction of light with phonons of the acoustic branches close to the Brillouin zone center in reciprocal space, represents an effective experimental technique for the determination of elastic and elasto-optic Pockels' constants. In particular, from the phenomenological theory of Brillouin scattering, elasto-optic constants are given in terms of the intensities of Brillouin components.[2,3]

A microscopic modeling and understanding of this peculiar, fundamental, optical property of crystals is relevant to the fields of optics and microelectronics: photoelasticity, indeed, reduces the efficiency of α-quartz fiber Bragg gratings and deteriorates the resolution of pure silica optical lenses used to design transistors by photolithography.[4–6]

The usual anisotropy of crystalline compounds increases the information content of many physical properties: the dielectric constant becomes a second-rank tensor $\boldsymbol{\epsilon}$ and the phenomenon of birefringence may appear, which corresponds to light propagating with different speeds along different crystallographic directions.[7] The elasto-optic constants become the components of the fourth-rank Pockels' tensor $\mathbb{P}$, which linearly relates the inverse of the dielectric tensor $\boldsymbol{\epsilon}^{-1}$ to the second-rank elastic strain tensor $\boldsymbol{\eta}$. In general, Pockels' tensor has 21 independent components, which the specific symmetry of the system can further reduce to a minimum of three for cubic crystals.

From a fundamental viewpoint, in the 1960s and 1970s, a lot of attention has been devoted to the experimental characterization of the photoelasticity of very simple crystals as face-centered cubic alkali halides[8–10] such as MgO, NaCl, NaF, LiF, KCl, KBr, and KI, and cubic diamondlike semiconductors[8,11,12] such as Si, SiC, BN, AlN, GaN, and hexagonal beryl, α-CdS, α-ZnS, and ZnO.[13–15] Interesting features for technological applications and anomalies of the photoelastic behavior of solids are found in more complex crystals such as titanium oxide TiO_2 rutile,[16] barium titanate $BaTiO_3$ perovskite with critical polarization fluctuations effects,[17,18] potassium dihydrogen phosphate KH_2PO_4 with an anomalous Curie-Weiss temperature dependence,[19] silicate glasses,[20,21] α-quartz SiO_2,[22,23] etc. Since most of the peculiar aspects of photoelasticity manifest in relatively complex crystalline structures, it is expected that rather sophisticated theoretical calculations are necessary to confirm or even predict those features accurately.

The aim of this paper is the presentation of an accurate, fully automated, *ab initio* scheme for the simulation and prediction of photoelastic constants of crystals which is developed within the formalism of periodic boundary conditions, one-electron Hamiltonians [Hartree-Fock (HF) or Kohn-Sham (KS)] and uses atom-centered Gaussian-type function (GTF) basis sets (all-electron basis sets can easily be used). The most interesting features of the present implementation are as follows: (i) generality over space groups of symmetry; (ii) full exploitation of both point and translational symmetry of the crystal; (iii) the possibility of separating electronic and nuclear "clamped-ion" contributions; (iv) evaluation of the electronic contribution to the static dielectric tensor through an analytical coupled-perturbed HF or KS scheme (CPHF or CPKS, respectively); and (v) electric field frequency dependence of Pockels' tensor.

Few *ab initio* studies of the photoelasticity of crystals have been reported in the literature so far: Levine and coworkers have performed local-density-approximation (LDA) calculations, with a scissor correction, in the pseudopotential, plane-wave scheme, on silicon and GaAs;[24,25] Detraux and Gonze have reported a density-functional perturbation theory study of α-quartz within the LDA with a scissor correction;[26] the same formalism has been applied by Donadio *et al.* to the study of crystalline and amorphous silica;[27,28] and Hounsome *et al.* have used scissor-corrected LDA for computing the electric field dependence of the elasto-optic constants of silicon and diamond.[29]

The fully automated scheme presented here for computing elasto-optic tensors of crystals has been implemented in a development version of the CRYSTAL program[30,31] for solid-state quantum chemistry.[32] Once provided the space group of a given crystal, the program performs a full symmetry analysis and finds which elements of the fourth-rank tensor are independent and which deformations have to be actually considered in order to generate them all. Among other advantages, this scheme allows for the use of a large variety of density-functional theory (DFT) functionals of different types: LDA, generalized gradient approximation (GGA) and hybrids, such as the popular B3LYP (Refs. 33 and 34) and PBE0 (Ref. 35) hybrids, with 20% and 25% of HF exchange, respectively.

The structure of the paper is as follows: In Sec. II, the algorithm for the automated computation of Pockels' tensor is illustrated along with the computational details and the methodology for computing dielectric properties. In Sec. III, the numerical stability of the proposed scheme is discussed and the effect of different classes of one-electron Hamiltonians explored with respect to experimental reference data, on a number of crystals of different symmetry. Conclusions are drawn in Sec. IV.

II. COMPUTATIONAL TECHNIQUES AND DETAILS

The elements of Pockels' elasto-optic fourth-rank tensor $\mathbb{P}$ (i.e., elasto-optic constants $\{p_{ijkl}\}$) are defined by the relation

$$\Delta\epsilon^{-1}_{ij} = \sum_{kl} p_{ijkl}\eta_{kl}. \tag{1}$$

In the above expression, $\Delta\boldsymbol{\epsilon}^{-1}$ is the difference between the inverse dielectric tensor of a strained and the unstrained equilibrium configuration; $i,j,k,l = x,y,z$ represent Cartesian directions. Formally, the dielectric tensor should read $\boldsymbol{\epsilon}(\boldsymbol{\eta})$ but the explicit dependence from the strain status of the system is omitted and made implicit, as a notation shortcut. In Eq. (1), $\boldsymbol{\eta}$ is the pure strain tensor,[36]

$$\boldsymbol{\eta} = \tfrac{1}{2}(\mathbf{C} - \mathbf{I}) \quad \text{with} \quad \mathbf{C} = \mathbf{E}^{\top}\mathbf{E}, \tag{2}$$

where $\mathbf{I}$ is the second-rank identity tensor and the position gradient $\mathbf{E}$ is defined in terms of the displacement gradient $\boldsymbol{\varepsilon}$ (not to be confused with the dielectric tensor $\boldsymbol{\epsilon}$) as

$$\mathbf{E} = \mathbf{I} + \boldsymbol{\varepsilon} \quad \text{or, in elements} \quad E_{ij} = \delta_{ij} + \varepsilon_{ij}. \tag{3}$$

From the relations above, we can express the Lagrangian finite strain parameters $\{\eta_{ij}\}$ in terms of deformation parameters $\{\varepsilon_{ij}\}$ as follows:

$$\eta_{ij} = \frac{1}{2}\left[\varepsilon_{ij} + \varepsilon_{ji} + \sum_{\lambda}\varepsilon_{\lambda i}\varepsilon_{\lambda j}\right]. \tag{4}$$

While $\boldsymbol{\varepsilon}$ has not been assumed to be symmetric, $\boldsymbol{\eta}$ is symmetric by construction, describes only pure strains, and vanishes when the deformation described by $\boldsymbol{\varepsilon}$ is a pure rotation. Given certain deformation parameters $\{\varepsilon_{ij}\}$, several deformations of different amplitude a (with a being a dimensionless parameter) can be defined according to $\boldsymbol{\varepsilon}(a) = a\boldsymbol{\varepsilon}$. As a consequence, $\boldsymbol{\eta} \to \boldsymbol{\eta}(a)$ and $\boldsymbol{\epsilon} \to \boldsymbol{\epsilon}(a)$.

Both the inverse dielectric tensor $\boldsymbol{\epsilon}^{-1}$ and the pure strain tensor $\boldsymbol{\eta}$ are symmetric; thus $\mathbb{P}$, in general, exhibits 21 independent elements due to these possible permutations among its indices: $(i \leftrightarrow j)$, $(k \leftrightarrow l)$, and $(ij \leftrightarrow kl)$. If Voigt's notation is used, according to which $v,u = 1,\ldots,6$ ($1 = xx$, $2 = yy$, $3 = zz$, $4 = yz$, $5 = xz$, $6 = xy$),[1] then Pockels' tensor becomes a 6×6 matrix whose elements can be deduced from Eq. (1) as

$$p_{vu} = \frac{\partial\Delta\epsilon^{-1}_{v}}{\partial\,\eta_{u}}. \tag{5}$$

For each independent strain η_u, the dielectric tensor $\boldsymbol{\epsilon}$ is computed for different values of a in such a way that the elasto-optic constants can be obtained by finite differences from Eq. (5).

A. The automated scheme

Let us sketch the fully automated procedure that we have implemented in the CRYSTAL program for the calculation of elasto-optic constants of crystals of any space group:

(1) Lattice parameters and atomic positions of the crystal structure are accurately optimized with tight convergence tolerances (see Sec. II C for their values).

(2) A single-point self-consistent-field (SCF) calculation is performed on the optimized unstrained structure. The equilibrium dielectric tensor $\boldsymbol{\epsilon}(0)$ is also computed with the CPHF/KS scheme, briefly discussed in Sec. II B.

(3) A symmetry analysis is performed in order to find the minimal set of deformations, out of a maximum of six, which have to be explicitly applied in order to get all the independent elasto-optic constants.

(4) Pick one independent deformation:

(a) The deformation is applied and the residual symmetry determined. N_s strained configurations are defined according to a strain amplitude a.

(b) For each strained configuration, the atomic positions are relaxed (default option) or not, depending on whether one wants to go beyond the "clamped-ion" approximation or not. An SCF + CPHF/KS calculation is then performed for computing the dielectric tensor $\boldsymbol{\epsilon}(a)$.

(c) From the set of dielectric tensors $\{\boldsymbol{\epsilon}(a)\}$, the N_s tensors $\Delta\boldsymbol{\epsilon}^{-1}(a) = \boldsymbol{\epsilon}^{-1}(a) - \boldsymbol{\epsilon}^{-1}(0)$ are computed and fitted with singular-value-decomposition routines; their first derivatives are determined numerically and coincide with the elasto-optic constants according to Eq. (5).

(5) Go back to point 4 or exit if all the independent deformations have been considered.

By default, $N_s = 2$, corresponding to one "expanded" and one "contracted" configuration with a strain amplitude $a = 0.015$.

B. The dielectric tensor

The electronic contribution to the static dielectric tensor, at zero electric field frequency $\omega = 0$, is evaluated through a CPHF/KS scheme[37] adapted for periodic systems.[38] From an experimental viewpoint, it corresponds to the dielectric response of the crystal measured for sufficiently high frequencies of the applied electric field to make nuclear contributions negligible, but not high enough for generating electronic

excitations. CPHF/KS is a perturbative, self-consistent method that focuses on the description of the relaxation of the crystalline orbitals under the effect of an external electric field. The perturbed wave function is then used to calculate the dielectric properties as energy derivatives. Further details about the method and its implementation in the CRYSTAL program can be found elsewhere,[39–41] as well as some recent examples of its application.[42–46] The electronic dielectric tensor of a three-dimensional (3D) crystal is obtained from the polarizability $\boldsymbol{\alpha}$ as

$$\boldsymbol{\epsilon}^{\mathrm{el}} = 1 + \frac{4\pi}{V}\boldsymbol{\alpha}^{\mathrm{el}} , \tag{6}$$

where V is the cell volume. With such a scheme, the explicit dependence of the polarizability and dielectric tensors from the electric field frequency ω can be computed as well. Nuclear contributions to the dielectric tensor could be introduced as follows:

$$\epsilon_{ij} = \epsilon_{ij}^{\mathrm{el}} + \epsilon_{ij}^{\mathrm{nuc}} = \epsilon_{ij}^{\mathrm{el}} + \frac{4\pi}{V}\sum_{p}\frac{Z_{p,i}Z_{p,j}}{\nu_p^2} , \tag{7}$$

where the summation runs over the phonon modes, ν_p is the phonon frequency of mode p, and $\mathbf{Z}_p$ is the mass-weighted mode effective Born vector.[47] Atomic Born effective tensors and mode effective Born vectors are computed through a Berry-phase approach[48,49] in the CRYSTAL program.

We recall that elasto-optic constants can be decomposed into purely electronic "clamped-ion" and nuclear "internal-strain" contributions, as for the dielectric tensor, $p_{vu} = p_{vu}^{\mathrm{el}} + p_{vu}^{\mathrm{nuc}}$; the latter measures the photoelastic effect due to relaxation of the relative positions of atoms induced by the strain[50,51] and can be computed simply by optimizing the atomic positions within the strained cell.

C. Computational parameters

All the calculations reported in the manuscript are performed with the program CRYSTAL for *ab initio* quantum chemistry of the solid state.[30,31] All-electron atom-centered GTF basis sets of triple-ζ valence quality, augmented by a polarization function (TZVP), are adopted.[52] Four different one-electron Hamiltonians have been considered as representatives of different classes: the reference HF, a local density,[53] and a generalized gradient, namely Perdew-Burke-Ernzerhof (PBE),[54] approximation to the DFT and the hybrid PBE0 functional.

In CRYSTAL, the truncation of infinite lattice sums is controlled by five thresholds, which are here set to 10,10,10,12, 24. Reciprocal space is sampled according to a sublattice with shrinking factor of 10. The DFT exchange-correlation contribution is evaluated by numerical integration over the cell volume. Radial and angular points of the atomic grid are generated through Gauss-Legendre and Lebedev quadrature schemes using an accurate predefined pruned grid. The accuracy in the integration procedure can be estimated by evaluating the error associated with the integrated electronic charge density in the unit cell versus the total number of electrons per cell: $1 \times 10^{-5}|e|$ out of a total number of 90 electrons per cell for α-quartz, for instance. Further details about the grid generation and its influence on the accuracy and cost of the calculations can be found elsewhere.[55–57] The convergence threshold on energy for the SCF step of the calculations is set to 10^{-10} hartree.

Equilibrium or strained configurations are optimized by use of analytical energy gradients with respect to both atomic coordinates and unit-cell parameters or atomic coordinates only, respectively.[58–60] A quasi-Newtonian technique is used, combined with the BFGS (Broyden-Fletcher-Goldfarb-Shanno) algorithm for Hessian updating.[61–64] Convergence has been checked on both gradient components and nuclear displacements; the corresponding tolerances on their root mean square are chosen 10 times more severe than the default values for simple optimizations: 0.00003 and 0.00012 atomic units (a.u.), respectively.

III. RESULTS AND DISCUSSION

A. Numerical stability

This section is devoted to the discussion of the numerical stability of the automated algorithm illustrated in Sec. II A for the computation of elasto-optic tensors of crystals, with respect to its two internal parameters, N_s and a. We recall here that N_s represents the number of strained configurations used per each independent deformation while a defines the strain amplitude. As we shall discover below, the algorithm proves extremely stable with respect to these two parameters. Three prototypical crystals are here considered that are cubic NaCl, cubic silicon, and trigonal α-quartz. The effect on the dielectric tensor of a number of general computational parameters such as the shrinking factor, the two-electron integrals tolerances, the DFT integration grid, etc., is not explicitly explored here; we rather prefer to address the reader to Refs. 39–41, and 65, where these effects are discussed with regard to a number of crystals.

In order to discuss the numerical stability of elasto-optic constants, we compare them with elastic constants (i.e., energy second derivatives with respect to pairs of strains) which can be computed with CRYSTAL using an algorithm with the same general structure as that proposed in Sec. II A.[66]

Crystalline silicon and NaCl have three independent elasto-optic (p_{11}, p_{12}, and p_{44}) and elastic (C_{11}, C_{12}, and C_{44}) constants that are reported in Table I, as computed at PBE level, as a function of the number N_s of strained configurations per independent deformation. The strain amplitude used is here $a = 0.015$. It is clearly seen how insensitive elasto-optic constants are to the parameter N_s; when more than two strained configurations are considered, the photoelastic results are perfectly converged. This is not the case for elastic constants that, although in turn are rather stable, show a somehow larger dependence from N_s (see C_{11} for NaCl and C_{44} for silicon, for instance, which still changes by 0.5% and 0.3% when passing from $N_s = 3$ to $N_s = 6$, respectively).

The six independent elastic and elasto-optic constants of α-quartz are also reported in Table I as a function of N_s; the same considerations made for NaCl and crystalline silicon hold true also in this case. It is again observed that when three strained configurations are used, elasto-optic constants are already converged in all cases but p_{11}, which converges to the value of 0.161 at $N_s = 4$.

In order to further investigate the numerical stability of Pockels' constants with respect to the number N_s of strained

TABLE I. Elasto-optic and elastic constants of NaCl, silicon, and α-quartz, computed at PBE level, as a function of the number N_s of strained configurations per independent deformation. The strain amplitude is $a = 0.015$.

	NaCl					Silicon					α-Quartz				
N_s	2	3	4	5	6	2	3	4	5	6	2	3	4	5	6
p_{11}	0.120	0.119	0.119	0.119	0.119	−0.112	−0.107	−0.107	−0.107	−0.107	0.152	0.160	0.161	0.161	0.161
p_{12}	0.163	0.166	0.166	0.166	0.166	0.004	0.010	0.010	0.010	0.010	0.295	0.297	0.297	0.297	0.297
p_{13}	0.163	0.166	0.166	0.166	0.166	0.004	0.010	0.010	0.010	0.010	0.298	0.298	0.298	0.297	0.298
p_{33}	0.120	0.119	0.119	0.119	0.119	−0.112	−0.107	−0.107	−0.107	−0.107	0.106	0.107	0.107	0.107	0.107
p_{14}	0.000	0.000	0.000	0.000	0.000	0.000	0.000	0.000	0.000	0.000	−0.060	−0.059	−0.059	−0.059	−0.059
p_{44}	−0.007	−0.007	−0.007	−0.007	−0.007	−0.054	−0.054	−0.054	−0.054	−0.054	−0.089	−0.089	−0.089	−0.089	−0.089
C_{11}	54.730	60.526	60.603	61.132	60.297	148.092	150.494	150.472	150.334	150.535	88.011	88.990	89.155	89.796	88.429
C_{12}	12.487	12.639	12.646	12.685	12.621	58.390	61.487	61.506	61.626	61.431	12.492	13.980	14.125	14.298	14.144
C_{13}	12.487	12.639	12.646	12.685	12.621	58.390	61.487	61.506	61.626	61.431	19.754	20.488	20.604	21.053	20.283
C_{33}	54.730	60.526	60.603	61.132	60.297	148.092	150.494	150.472	150.334	150.535	111.414	113.999	114.134	114.931	113.740
C_{14}	0.000	0.000	0.000	0.000	0.000	0.000	0.000	0.000	0.000	0.000	13.734	12.333	12.350	12.347	12.469
C_{44}	12.691	12.691	12.709	12.831	12.665	66.937	66.950	66.979	67.164	66.755	58.702	58.701	58.656	58.342	58.838

configurations, we report in Fig. 1 the quantities $\Delta\epsilon^{-1}_{xx}$ and $\Delta\epsilon^{-1}_{yz}$ for NaCl, crystalline silicon, and α-quartz as a function of the strain amplitude a along η_{xx} and along η_{yz} in the left and right panels, respectively. From Eq. (5) we can easily see how the slopes (i.e., first derivatives) of the curves in the figure represent elasto-optic constants p_{11} and p_{44}. From inspection of the figure, it can be noticed that data in the right panel behave much more linearly than the corresponding data in the left panel; as a consequence, the corresponding slopes turn out to be more stable with respect to the number of points considered. We can check in Table I, indeed, that the p_{44} constant of the three crystals is very stable with respect to N_s, showing converged values already at $N_s = 2$. This constant is negative for all three crystals, with a very small value of –0.007 for NaCl, a larger value of –0.054 for silicon, and the largest value, –0.089, for α-quartz, as the figure confirms. Data in the left panel are a bit less linearly distributed and thus the corresponding elasto-optic constant p_{11} is found to be slightly more dependent on N_s, being converged at $N_s = 3$ for NaCl and silicon and $N_s = 4$ for α-quartz. In this case, p_{11} is negative, –0.107, for silicon and positive for NaCl, 0.119, and α-quartz, 0.161. The higher linearity of the right panel data is most certainly due to the fact that the deformation η_{yz} preserves the cell volume while η_{xx} does not.

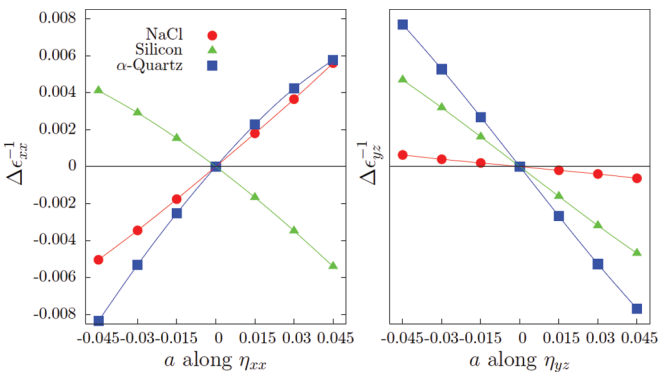

FIG. 1. (Color online) $\Delta\epsilon^{-1}_{xx}$ as a function of the strain amplitude a along η_{xx} (left panel), and $\Delta\epsilon^{-1}_{yz}$ as a function of the strain amplitude a along η_{yz} (right panel), for NaCl (red circles), crystalline silicon (green triangles), and α-quartz (blue squares), as computed at PBE level. The slopes of these curves give elasto-optic constants p_{11} and p_{44} in the left and right panels, respectively.

The effect of the adopted strain amplitude a is investigated in Table II, where elastic and elasto-optic constants of NaCl, silicon, and α-quartz, computed at PBE level over $N_s = 3$ strained configurations, are reported for three values of a (0.005, 0.01, and 0.015). From the table it can be seen how independent elasto-optic constants are from a. Only the first four constants of α-quartz show very slight oscillations in their values. Elastic constants are less stable with respect to this parameter, showing larger oscillations: up to 1.3% for C_{11} of NaCl, 0.6% for C_{13} of crystalline silicon, and 2.3% for C_{13} of α-quartz.

The two parameters N_s and a are obviously correlated. We note that if a larger strain range is considered, where an increased nonlinearity appears (refer again to Fig. 1), then a larger number of points N_s should be considered so as to include nonlinear terms in the fitting procedure.

B. The effect of the Hamiltonian

This section is devoted to the analysis of the effect of the adopted one-electron Hamiltonian on computed elasto-optic constants of crystals. From previous applications of the CPHF/KS method to different crystals, we know that the generalized-gradient approximation to the DFT usually provides the best agreement with experimental dielectric tensors, much better than HF and even better than hybrid schemes.[39–41,65] Nevertheless, elasto-optic constants are not directly proportional to the dielectric constants but rather to their variation with respect to finite mechanical strains. It is indeed interesting to see whether the same hierarchy of one-electron Hamiltonians holds true or not when passing from dielectric to elasto-optic constants.

In order to do so, a set of eight crystalline systems of different symmetries is here considered for which accurate experimental data are available to compare with: simple cubic sodium chloride NaCl, lithium fluoride LiF, magnesium oxide MgO and potassium chloride KCl; cubic silicon and diamond; trigonal SiO_2 α-quartz; and tetragonal TiO_2 rutile.

TABLE II. Elasto-optic and elastic constants of NaCl, silicon, and α-quartz, computed at PBE level, as a function of the strain amplitude a. The number N_s of strained configurations considered is 3.

	NaCl			Silicon			α-Quartz		
a	0.005	0.01	0.015	0.005	0.01	0.015	0.005	0.01	0.015
p_{11}	0.119	0.119	0.119	−0.107	−0.107	−0.107	0.160	0.159	0.160
p_{12}	0.166	0.166	0.166	0.010	0.010	0.010	0.297	0.297	0.297
p_{13}	0.166	0.166	0.166	0.010	0.010	0.010	0.298	0.297	0.298
p_{33}	0.119	0.119	0.119	−0.107	−0.107	−0.107	0.107	0.106	0.107
p_{14}	0.000	0.000	0.000	0.000	0.000	0.000	−0.059	−0.059	−0.059
p_{44}	−0.007	−0.007	−0.007	−0.054	−0.054	−0.054	−0.089	−0.089	−0.089
C_{11}	60.465	61.056	60.246	150.502	150.350	150.554	88.914	89.689	88.691
C_{12}	12.636	12.681	12.618	61.476	61.610	61.428	13.861	14.229	14.043
C_{13}	12.636	12.681	12.618	61.476	61.610	61.428	20.506	20.977	20.550
C_{33}	60.465	61.056	60.246	150.502	150.350	150.554	113.959	114.807	113.783
C_{14}	0.000	0.000	0.000	0.000	0.000	0.000	12.297	12.343	12.365
C_{44}	12.679	12.815	12.671	66.942	67.132	66.737	58.638	58.352	58.836

Four one-electron Hamiltonians are considered: the reference HF method, a LDA and the PBE generalized-gradient functionals of the DFT, and the hybrid PBE0 scheme. The dielectric and elasto-optic constants of the above-mentioned set of crystals, as computed with these four Hamiltonians, are reported in Table III along with the corresponding experimental values. Elasto-optic constants are obtained by using three strained configurations ($N_s = 3$) and a strain amplitude $a = 0.015$.

Let us first consider the dielectric constants. From the table it is clearly seen that HF performs very poorly by systematically underestimating $\epsilon^{\rm el}$ with deviations from the experimental values as large as 33% for crystalline silicon and 41% for NaCl. The PBE0 hybrid scheme, with its 25% of HF exchange, significantly ameliorates the dielectric description with respect to HF but still underestimates the dielectric response. Pure DFT functionals, LDA and PBE, predict the dielectric tensors generally quite close to the experimental ones, even if slightly overestimated, with PBE being a bit better than LDA in this respect.

With regard to elasto-optic constants, similar considerations can be done by looking at the data in Table III. An overall index is reported in the last row of the table that is $|\Delta p| = \sum |p^{\rm calc} - p^{\rm exp}|$, where the sum runs over all the elasto-optic constants of the eight crystals in the table. The sum of the absolute values of the experimental constants is 50.5. The HF method is definitely not suitable for computing such quantities with an overall deviation from the experimental values of 18.0. The hybrid PBE0 scheme gives an overall deviation of 6.2. Again, pure DFT functionals, LDA and especially PBE, are providing the best agreement with the experimental values with $|\Delta p|$ of 4.1 and 1.9, respectively. Thus the photoelastic description provided by a generalized-gradient functional improves by a factor of 2 upon that of a simple local-density functional.

It is worth mentioning that, due to relatively large experimental uncertainties associated with the measured elasto-optic values (as large as 100% in some cases),[16] the agreement between calculated and measured values is not expected to be perfect for photoelastic constants with small absolute values (i.e., $|p| < 0.05$). In this respect, see the discussion in Sec. III C about the determination of the absolute values of elasto-optic constants of the simple crystal of MgO.

In order to illustrate which is the nuclear contribution to the total elasto-optic constants of the set of crystals we have been considering so far, in Table III we also report the purely electronic "clamped-ion" contributions (values in parentheses) as obtained at PBE level by keeping fixed atomic positions in the strained configurations. From the comparison of the third and fourth data columns in the table, we see how, as expected from symmetry considerations, for simple cubic crystals such as NaCl, LiF, MgO, and KCl the nuclear contribution is null. Crystalline silicon and diamond are characterized by a nonvanishing nuclear term in the elasto-optic constant p_{44} only, whereas α-quartz and rutile show a very large nuclear contribution in all the independent constants. When nuclear contributions are included, some elasto-optic constants vary an order of magnitude (see p_{13} in α-quartz) while for others a change in sign even occurs, such as for p_{11} and p_{33} for α-quartz and p_{11} for rutile.

C. Comparing with experiments: The MgO case

At the end of the previous section, we were mentioning that a perfect agreement between theory and experiments cannot be expected for such a property as photoelasticity due to the relatively high error bars associated with the experimental values. In order to further investigate which are the actual reasons for this uncertainty, we shall consider the very simple case of the MgO cubic crystal. In Table IV we review the existing experimental studies on MgO, along with our results. From the analysis of the table, it is clearly seen how scattered experimental elasto-optic constants are, especially so for p_{11} and p_{12}. In the table we also report the quantity $(p_{11} - p_{12})$, because this combination, along with p_{44}, can be directly deduced from accurate birefringence experiments (such as using the Babinet compensator). Indeed, experimental values for $(p_{11} - p_{12})$ and p_{44} show a much better agreement among them. The experimental techniques (for instance, Mueller's ultrasonic method) used for determining the p_{11}/p_{12} ratio are subject to serious errors. As a consequence, it is not surprising

TABLE III. Dielectric and elasto-optic constants of several crystals as computed with different one-electron Hamiltonians and compared with the experiment. In parentheses, the electronic "clamped-ion" contribution to PBE elasto-optic constants is also reported. See text for definition of $|\Delta p|$.

	HF	LDA	PBE		PBE0	EXP.
NaCl						
ϵ^{el}	1.395	2.615	2.430		2.330	2.380[8]
p_{11}	0.308	0.077	0.119	(0.119)	0.136	0.115[9]
p_{12}	0.194	0.157	0.166	(0.166)	0.185	0.161[9]
p_{44}	−0.022	−0.002	−0.007	(−0.007)	−0.005	−0.011[9]
LiF						
ϵ^{el}	1.448	2.042	1.975		1.894	1.940[8]
p_{11}	0.231	−0.044	−0.026	(−0.026)	0.000	0.020[67]
p_{12}	0.219	0.139	0.136	(0.136)	0.155	0.130[67]
p_{44}	−0.045	−0.051	−0.054	(−0.054)	−0.055	−0.064[67]
MgO						
ϵ^{el}	1.848	3.077	3.097		2.868	3.020[10]
p_{11}	−0.127	−0.218	−0.213	(−0.213)	−0.195	−0.210[68]
p_{12}	0.091	0.013	0.015	(0.015)	0.037	0.040[68]
p_{44}	−0.147	−0.075	−0.078	(−0.078)	−0.083	−0.100[68]
KCl						
ϵ^{el}	1.908	2.396	2.199		2.125	2.220[8]
p_{11}	0.289	0.230	0.257	(0.257)	0.272	0.233[9]
p_{12}	0.202	0.175	0.181	(0.181)	0.192	0.169[9]
p_{44}	−0.044	−0.035	−0.046	(−0.046)	−0.044	−0.026[9]
Silicon						
ϵ^{el}	7.952	10.468	12.087		10.409	11.830[12]
p_{11}	−0.163	−0.111	−0.107	(−0.107)	−0.109	−0.094[12]
p_{12}	0.000	0.020	0.010	(0.010)	0.021	0.017[12]
p_{44}	−0.100	−0.056	−0.054	(−0.093)	−0.055	−0.051[12]
Diamond						
ϵ^{el}	4.974	5.668	5.749		5.443	5.819[69]
p_{11}	−0.302	−0.264	−0.270	(−0.270)	−0.268	−0.248[70]
p_{12}	0.056	0.076	0.073	(0.073)	0.072	0.044[70]
p_{44}	−0.214	−0.162	−0.175	(−0.189)	−0.175	−0.172[70]
α-Quartz						
ϵ^{el}_{xx}	1.935	2.453	2.347		2.209	2.356[26]
ϵ^{el}_{zz}	1.950	2.497	2.384		2.238	2.383[26]
p_{11}	0.168	0.203	0.160	(−0.202)	0.173	0.160[23]
p_{12}	0.304	0.289	0.297	(0.073)	0.304	0.270[23]
p_{13}	0.313	0.299	0.298	(0.029)	0.312	0.270[23]
p_{33}	0.148	0.112	0.107	(−0.197)	0.126	0.100[23]
p_{14}	−0.047	−0.052	−0.059	(−0.010)	−0.055	−0.047[23]
p_{44}	−0.066	−0.075	−0.089	(−0.166)	−0.081	−0.079[23]
Rutile						
ϵ^{el}_{xx}	3.404	7.476	7.266		5.478	6.840[16]
ϵ^{el}_{zz}	3.934	9.054	9.027		6.684	8.430[16]
p_{11}	0.008	0.020	0.038	(−0.042)	0.033	0.012[16]
p_{12}	0.235	0.137	0.166	(0.104)	0.204	0.144[16]
p_{13}	−0.011	−0.094	−0.130	(−0.195)	−0.107	−0.140[16]
p_{33}	−0.040	−0.040	−0.075	(−0.058)	−0.068	−0.057[16]
p_{44}	−0.023	−0.004	0.000	(0.039)	−0.010	×
p_{66}	−0.067	−0.064	−0.082	(−0.082)	−0.087	−0.062[16]
$\|\Delta p\|$	18.0	4.1	1.9	(3.2)	6.2	–

to find that the individual values of p_{11} and p_{12} deduced by several workers are so different from one another. In particular, even the sign of p_{12} is not uniquely determined, with values ranging from –0.08 to 0.04.

TABLE IV. Elasto-optic constants of the MgO crystal as experimentally measured by various workers, compared with the results of the present study.

	$p_{11}-p_{12}$	p_{44}	p_{11}	p_{12}
Giardini and Poindexter[68]	−0.25	−0.10	−0.21	+0.04
Vedam and Schmidt[10]	−0.248	×	−0.259	−0.011
Cardona *et al.*[71]	−0.24	×	−0.3	−0.08
Krishna Rao *et al.*[72]	−0.24	−0.105	−0.31	−0.07
West and Makas[73]	−0.253	−0.096	×	×
Present work LDA	−0.231	−0.075	−0.218	+0.013
Present work PBE	−0.228	−0.078	−0.213	+0.015

Moreover, even if experiments are supposed to measure the variation of the *static* dielectric tensor (i.e., at zero electric field frequency, $\omega = 0$, $\lambda = \infty$), they are performed at finite electric field wavelengths which may not correspond to the static limit. The experiments reviewed in Table IV have been carried out in the wavelength range from 540 to 589.3 nm. In Fig. 2, we report the three independent elasto-optic constants of MgO, computed at PBE level, as a function of the electric field wavelength λ. From its inspection we can see that while p_{44} is almost wavelength independent, p_{11} and p_{12} show a clear dependence from λ, slowly converging to the static limit values above 1000 nm. In particular, the value of p_{12} is found to pass from negative to positive at around 550 nm. Dashed vertical lines in the figure identify the experimental range of adopted electric field wavelengths: both p_{11} and p_{12} are still changing in that range. This aspect is particularly crucial for the determination of p_{12} since, within such a range, it is even changing sign.

The reason is now clear for the uncertainty in the experimental determination of the value of p_{12}. From this simple example, the usefulness, and complementarity with experiments, of the theoretical *ab initio* scheme presented here

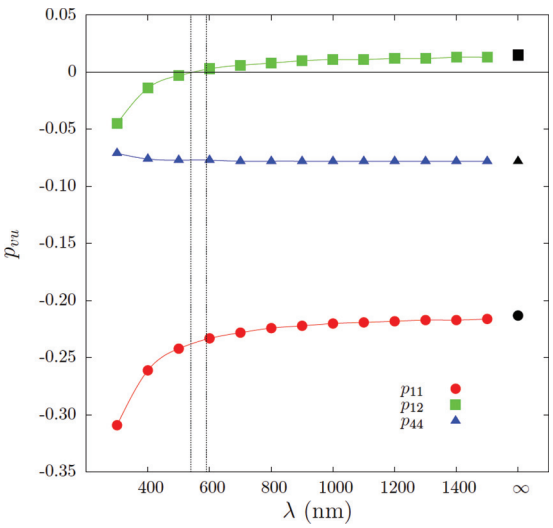

FIG. 2. (Color online) The three independent elasto-optic constants of the MgO crystal as computed at PBE level as a function of the electric field wavelength λ; continuous lines are intended as visual guides. The infinite wavelength results are also shown. Dashed vertical lines represent the experimental wavelength range.

for the investigation and interpretation of photoelasticity of crystals is revealed.

IV. CONCLUSIONS

A fully automated *ab initio* scheme for the computation of elasto-optic constants of crystals is presented which is general, takes advantage of a complete symmetry analysis of the system, works within periodic boundary conditions, and exploits both translational and point symmetry. Several one-electron Hamiltonians can be used to compute Pockels' fourth-rank tensor. An analytical coupled-perturbed Hartree-Fock/Kohn-Sham technique is used for the calculation of the dielectric tensor of crystals under finite strains. The numerical stability and accuracy of the scheme are discussed. Elasto-optic constants are found to be very stable with respect to internal parameters of the approach proposed.

Pure density-functional theory functionals are providing the best description of the photoelastic properties of crystals, if compared with Hartree-Fock or even hybrid schemes. In particular, generalized-gradient functionals are found to improve the agreement with experiments by a factor of 2 with respect to simple local-density functionals, commonly reported in the literature so far. In order to help in the interpretation of the photoelastic response of crystals, the separation of total into electronic and nuclear "clamped-ion" contributions has been implemented. Moreover, the possibility of computing the electric field frequency dependence of elasto-optic constants is shown to constitute a valuable tool when compared with their experimental counterparts.

The scheme proposed here can be successfully applied to crystals of any symmetry and size. We are currently investigating the photoelastic properties of six garnet end members (namely, pyrope, almandine, spessartine, andradite, uvarovite, and grossular) and their solid solutions, with 80 atoms in the primitive cell. The results of such an investigation will be reported in a forthcoming paper.

ACKNOWLEDGMENT

Dr. Roberto Orlando is kindly acknowledged for useful discussions.

*alessandro.erba@unito.it

[1] J. F. Nye, *Physical Properties of Crystals* (Oxford University Press, Oxford, 1957).
[2] H. Z. Cummins and P. E. Schoen, in *Laser Handbook*, edited by F. T. Arecchi and E. O. Schulz-Dubois (North-Holland Publishing Co., Amsterdam, 1972), p. 1029.
[3] D. Landheer, H. E. Jackson, R. A. McLaren, and B. P. Stoicheff, Phys. Rev. B **13**, 888 (1976).
[4] H. Limberger, P. Fonjallaz, R. Salathe, and F. Cochet, Appl. Phys. Lett. **68**, 3069 (1996).
[5] R. Schenker and W. Oldman, J. Appl. Phys. **82**, 1065 (1997).
[6] N. F. Borrelli, C. Smith, D. C. Allan, and T. P. Seward, J. Opt. Soc. Am. B **14**, 1606 (1997).
[7] L. D. Landau and E. M. Lifshitz, *Electrodynamics of Continuous Media*, Course of Theoretical Physics Vol. 8 (Pergamon Press, Oxford, 1960).
[8] K. G. Aggarwal and B. Szigeti, J. Phys. C: Solid State Phys. **3**, 1097 (1970).
[9] L. Benckert and G. Bäckström, Phys. Rev. B **8**, 5888 (1973).
[10] K. Vedam and E. D. D. Schmidt, Phys. Rev. **146**, 548 (1966).
[11] S. Y. Davydov and S. K. Tikhonov, Semiconductors **31**, 698 (1997).
[12] D. K. Biegelsen, Phys. Rev. Lett. **32**, 1196 (1974).
[13] K. Vedam and T. A. Davis, Phys. Rev. **181**, 1196 (1969).
[14] T. Azuhata, M. Takesada, T. Yagi, A. Shikanai, S. Chichibu, K. Torii, A. Nakamura, T. Sota, G. Cantwell, D. B. Eason *et al.*, J. Appl. Phys. **94**, 968 (2003).
[15] R. Bercowicz and T. Skettrup, Phys. Rev. B **11**, 2316 (1975).
[16] M. H. Grimsditch and A. K. Ramdas, Phys. Rev. B **14**, 1670 (1976).
[17] M. G. Cohen, M. DiDomenico, and S. H. Wemple, Phys. Rev. B **1**, 4334 (1970).
[18] M. Zgonik, P. Bernasconi, M. Duelli, R. Schlesser, P. Günter, M. H. Garrett, D. Rytz, Y. Zhu, and X. Wu, Phys. Rev. B **50**, 5941 (1994).
[19] E. M. Brody and H. Z. Cummins, Phys. Rev. Lett. **23**, 1039 (1969).
[20] J. Schroeder, J. Non-Cryst. Solids **40**, 549 (1980).
[21] P. Benassi, V. Mazzacurati, G. Ruocco, and G. Signorelli, Phys. Rev. B **48**, 5987 (1993).
[22] T. Narasimhamurty, J. Opt. Soc. Am. **59**, 682 (1969).
[23] L. Levien, C. Prewitt, and D. Weidner, Acta Metall. Mater. **65**, 920 (1980).
[24] Z. H. Levine, H. Zhong, S. Wei, D. C. Allan, and J. W. Wilkins, Phys. Rev. B **45**, 4131 (1992).
[25] J. E. Raynolds, Z. H. Levine, and J. W. Wilkins, Phys. Rev. B **51**, 10477 (1995).
[26] F. Detraux and X. Gonze, Phys. Rev. B **63**, 115118 (2001).
[27] D. Donadio, M. Bernasconi, and F. Tassone, Phys. Rev. B **68**, 134202 (2003).
[28] D. Donadio, M. Bernasconi, and F. Tassone, Phys. Rev. B **70**, 214205 (2004).
[29] L. S. Hounsome, R. Jones, M. J. Shaw, and P. R. Briddon, Phys. Status Solidi **203**, 3088 (2006).
[30] R. Dovesi, V. R. Saunders, C. Roetti, R. Orlando, C. M. Zicovich-Wilson, F. Pascale, K. Doll, N. M. Harrison, B. Civalleri, I. J. Bush, Ph. D'Arco, and M. Llunell, *CRYSTAL09 User's Manual*, Università di Torino, Torino (2010), http://www.crystal.unito.it.
[31] R. Dovesi, R. Orlando, B. Civalleri, C. Roetti, V. R. Saunders, and C. M. Zicovich-Wilson, Z. Kristallogr. **220**, 571 (2005).
[32] The present implementation of the fully automated scheme for the calculation of photoelasticity of crystals will constitute a new feature of the next release of the program, namely, CRYSTAL13.
[33] A. D. Becke, J. Chem. Phys. **98**, 5648 (1993).
[34] C. Lee, W. Yang, and R. G. Parr, Phys. Rev. B **37**, 785 (1988).
[35] C. Adamo and V. Barone, J. Chem. Phys. **110**, 6158 (1999).
[36] A. A. Maradudin and E. Burstein, Phys. Rev. **164**, 1081 (1967).
[37] G. J. B. Hurst, M. Dupuis, and E. Clementi, J. Chem. Phys. **89**, 385 (1988).
[38] B. Kirtman, F. L. Gu, and D. M. Bishop, J. Chem. Phys. **113**, 1294 (2000).
[39] M. Ferrero, M. Rérat, R. Orlando, and R. Dovesi, J. Comput. Chem. **29**, 1450 (2008).
[40] M. Ferrero, M. Rérat, R. Orlando, and R. Dovesi, J. Chem. Phys. **128**, 014110 (2008).

[41]M. Ferrero, M. Rérat, B. Kirtman, and R. Dovesi, J. Chem. Phys. **129**, 244110 (2008).
[42]A. Erba, M. Ferrabone, J. Baima, R. Orlando, M. Rérat, and R. Dovesi, J. Chem. Phys. **138**, 054906 (2013).
[43]C. Carteret, M. De La Pierre, M. Dossot, F. Pascale, A. Erba, and R. Dovesi, J. Chem. Phys. **138**, 014201 (2013).
[44]A. Erba, Kh. E. El-Kelany, M. Ferrero, I. Baraille, and M. Rérat, Phys. Rev. B **88**, 035102 (2013).
[45]V. Lacivita, A. Erba, Y. Noël, R. Orlando, P. D'Arco, and R. Dovesi, J. Chem. Phys. **138**, 214706 (2013).
[46]J. Baima, A. Erba, M. Rérat, R. Orlando, and R. Dovesi, J. Phys. Chem. C **117**, 12864 (2013).
[47]X. Gonze and C. Lee, Phys. Rev. B **55**, 10355 (1997).
[48]R. Resta, Rev. Mod. Phys. **66**, 899 (1994).
[49]R. D. King-Smith and D. Vanderbilt, Phys. Rev. B **49**, 5828 (1994).
[50]G. Saghi-Szabo, R. E. Cohen, and H. Krakauer, Phys. Rev. Lett. **80**, 4321 (1998).
[51]A. Dal Corso, M. Posternak, R. Resta, and A. Baldereschi, Phys. Rev. B **50**, 10715 (1994).
[52]M. F. Peintinger, D. V. Oliveira, and T. Bredow, J. Comput. Chem. **34**, 451 (2013).
[53]S. H. Vosko, L. Wilk, and M. Nusair, Can. J. Phys. **58**, 1200 (1980).
[54]J. P. Perdew, K. Burke, and M. Ernzerhof, Phys. Rev. Lett. **77**, 3865 (1996).
[55]F. Pascale, C. M. Zicovich-Wilson, R. Orlando, C. Roetti, P. Ugliengo, and R. Dovesi, J. Phys. Chem. B **109**, 6146 (2005).
[56]M. Prencipe, F. Pascale, C. Zicovich-Wilson, V. Saunders, R. Orlando, and R. Dovesi, Phys. Chem. Min. **31**, 559 (2004).
[57]S. Tosoni, F. Pascale, P. Ugliengo, R. Orlando, V. R. Saunders, and R. Dovesi, Mol. Phys. **103**, 2549 (2005).
[58]K. Doll, Comput. Phys. Commun. **137**, 74 (2001).
[59]K. Doll, V. R. Saunders, and N. M. Harrison, Int. J. Quantum Chem. **82**, 1 (2001).
[60]B. Civalleri, P. D'Arco, R. Orlando, V. R. Saunders, and R. Dovesi, Chem. Phys. Lett. **348**, 131 (2001).
[61]C. G. Broyden, J. Inst. Math. Appl. **6**, 76 (1970).
[62]R. Fletcher, Comput. J **13**, 317 (1970).
[63]D. Goldfarb, Math. Comput. **24**, 23 (1970).
[64]D. F. Shanno, Math. Comput. **24**, 647 (1970).
[65]R. Orlando, V. Lacivita, R. Bast, and K. Ruud, J. Chem. Phys. **132**, 244106 (2010).
[66]W. F. Perger, J. Criswell, B. Civalleri, and R. Dovesi, Comput. Phys. Commun. **180**, 1753 (2009).
[67]D. W. Pohl and S. E. Schwarz, Phys. Rev. B **7**, 2735 (1973).
[68]A. A. Giardini and E. Poindexter, J. Opt. Soc. Am. **48**, 556 (1958).
[69]H. R. Philipp and E. A. Taft, Phys. Rev. **127**, 159 (1962).
[70]R. S. Leigh and B. Szigeti, J. Phys. C **3**, 782 (1970).
[71]M. Cardona, W. Paul, and H. Brooks, J. Phys. Chem. Solids **8**, 204 (1959).
[72]K. V. Krishna Rao and V. G. Krishna Murty, Acta Crystallogr. **17**, 788 (1964).
[73]C. D. West and A. B. Makas, J. Chem. Phys. **16**, 427 (1948).